ARTICLE

doi:10.1038/nature09553

Genetic dissection of an amygdala microcircuit that gates conditioned fear

Wulf Haubensak[1], Prabhat S. Kunwar[1]*, Haijiang Cai[1]*, Stephane Ciocchi[3]*, Nicholas R. Wall[4], Ravikumar Ponnusamy[5], Jonathan Biag[6], Hong-Wei Dong[6], Karl Deisseroth[7], Edward M. Callaway[4], Michael S. Fanselow[5], Andreas Lüthi[3] & David J. Anderson[1,2]

The role of different amygdala nuclei (neuroanatomical subdivisions) in processing Pavlovian conditioned fear has been studied extensively, but the function of the heterogeneous neuronal subtypes within these nuclei remains poorly understood. Here we use molecular genetic approaches to map the functional connectivity of a subpopulation of GABA-containing neurons, located in the lateral subdivision of the central amygdala (CEl), which express protein kinase C-δ (PKC-δ). Channelrhodopsin-2-assisted circuit mapping in amygdala slices and cell-specific viral tracing indicate that PKC-δ^+ neurons inhibit output neurons in the medial central amygdala (CEm), and also make reciprocal inhibitory synapses with PKC-δ^- neurons in CEl. Electrical silencing of PKC-δ^+ neurons *in vivo* suggests that they correspond to physiologically identified units that are inhibited by the conditioned stimulus, called CEl_{off} units. This correspondence, together with behavioural data, defines an inhibitory microcircuit in CEl that gates CEm output to control the level of conditioned freezing.

The amygdala is a medial temporal lobe region that is central to the acquisition and expression of Pavlovian conditioned fear[1–3]. The amygdala contains multiple anatomically defined nuclei[4]. Associative learning occurs largely in the lateral nucleus, whereas the central nucleus is thought to control the expression of fear[5,6]. However, the central nucleus contains at least three subnuclei (CEm, CEl and capsular central amygdala)[3,4] and multiple neuronal subtypes[7–10] whose role is poorly understood. A full understanding of amygdala function requires its dissection at the cellular level.

Here we have used genetic methods to investigate the functional connectivity and behavioural relevance of a GABAergic subpopulation within CEl[11–13], marked by the expression of PKC-δ. These neurons inhibit output neurons in CEm and also make reciprocal inhibitory connections with PKC-δ^- neurons within CEl. Genetic silencing[14,15] in conjunction with *in vivo* electrophysiology indicates that these neurons probably correspond to 'CEl_{off}' units identified in the accompanying paper[16] that are inhibited by the conditioned stimulus (CS). Taken together, these data define the functional connectivity and behavioural relevance of an inhibitory microcircuit within CEl[9,17] that gates output from CEm[12].

Properties of PKC-δ^+ neurons in CEl

We sought stable markers for subpopulations in the central nucleus[18,19], which could be used to genetically manipulate their activity *in vivo*[20–22]. PKC-δ marks about 50% of CEl GABAergic neurons (Fig. 1a–d and Supplementary Table 1). These neurons are distinct from those expressing corticotropin-releasing hormone[9] (Fig. 1e–g) or dynorphin[10] (Supplementary Fig. 1a–c), whereas about 40% express enkephalin[9] (Fig. 1h–j and Supplementary Table 1) and about 65% express the oxytocin receptor (Supplementary Fig. 1d–f and Supplementary Table 1), which is implicated in inhibitory gating of CEm[12].

We examined the electrophysiological properties of PKC-δ^+ neurons in acute amygdala slices. Because of their low spontaneous activity, spiking was evoked by the injection of depolarizing current. This analysis confirmed three types of neuron: late-firing, regular spiking and low-threshold bursting neurons[23–25] (Fig. 1k, l and Supplementary Table 2). Fills with neurobiotin and staining with antibodies, as well as recording from fluorescently labelled PKC-δ^+ neurons in transgenic mice (see below), indicated that most PKC-δ^+ neurons are late-firing (Fig. 1m, o and Supplementary Table 3), whereas the PKC-δ^- population contains both regular spiking and late-firing units (Fig. 1n, o and Supplementary Table 3). Thus, PKC-δ^+ neurons have relatively homogeneous electrophysiological properties (Supplementary Table 4; $P < 0.0001$, Fisher's exact test).

Functional connectivity of PKC-δ^+ neurons

To gain genetic access to PKC-δ^+ neurons, transgenic mice were generated[26] harbouring a bacterial artificial chromosome (BAC) expressing Cre recombinase and the α subunit of a cyan fluorescent protein (CFP)-tagged version of the *Caenorhabditis elegans* glutamate-sensitive chloride channel GluCl (ref. 27) (Fig. 2a), separated by an internal ribosome entry site (ires)[28]. Double labelling for GluClα–CFP and PKC-δ in these PKC-δ:GluClα-ires-Cre mice, as well as crossing to Cre-dependent *lacZ*-expressing reporter mice, revealed neuron-specific expression of the transgene (Fig. 2j–m) that correctly recapitulated the pattern of endogenous PKC-δ expression (Fig. 2b–i).

CEl is known to contain GABAergic neurons that project to CEm[7,12,29,30]. We traced the anterograde projections of PKC-δ^+ neurons to CEm by injecting the CEl of the transgenic mice with a Cre-dependent adeno-associated virus (AAV) encoding humanized *Renilla* green fluorescent protein[31] (hrGFP) (Fig. 3a–j). Recombination of injected AAVs was restricted to PKC-δ^+ neurons (Supplementary Fig. 2f–j). hrGFP$^+$ fibres derived from CEl projected to CEm (Fig. 3h, inset, and Fig. 3i, j), a result confirmed by retrograde tracing from CEm with the use of the B subunit of cholera toxin (CTB) (Fig. 3k, l). In all, $60.9 \pm 5.7\%$ (mean ± s.e.m., $n = 6$) of CTB$^+$ neurons in CEl were

[1]Division of Biology 216-76, California Institute of Technology, Pasadena, California 91125, USA. [2]Howard Hughes Medical Institute, California Institute of Technology, Pasadena, California 91125, USA. [3]Friedrich Miescher Institute for Biomedical Research, 4058 Basel, Switzerland. [4]Systems Neurobiology Laboratory, The Salk Institute for Biological Studies, La Jolla, California 92037, USA. [5]Department of Psychology and the Brain Research Institute, University of California, Los Angeles, Los Angeles, California 90095, USA. [6]Laboratory for Neuroimaging, University of California, Los Angeles, Los Angeles, California 90095, USA. [7]Department of Bioengineering, Stanford University, Stanford, California 94305, USA.
*These authors contributed equally to this work.

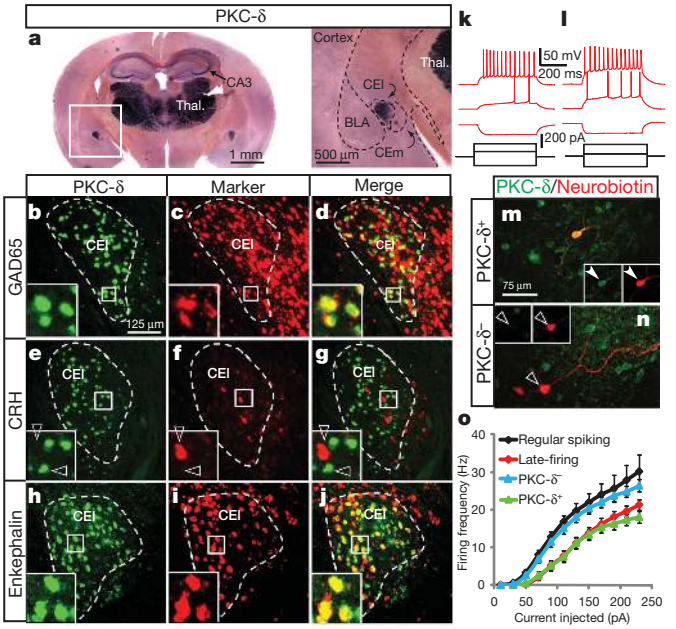

Figure 1 | Characterization of CEl PKC-δ$^+$ neurons. **a**, *In situ* hybridization for PKC-δ mRNA. CA3, hippocampus; thal., thalamus. The boxed area is shown at a higher magnification on the right. **b–j**, Double-label fluorescence *in situ* hybridization for PKC-δ mRNA and the indicated markers. The insets show enlargements of the boxed areas. Filled and open arrowheads indicate doubly labelled and singly labelled cells, respectively. CRH, corticotropin-releasing hormone. **k**, **l**, Whole-cell patch clamp recordings of late-firing (**k**) and regular spiking (**l**) neurons in acute amygdala slices. Voltage changes (red) produced by the respective current injections (black) are illustrated. Resting membrane potentials were adjusted to about −65 mV. **m**, **n**, Neurobiotin-filled CEl neurons recorded in **k** and **l**, respectively, after labelling with fluorescent streptavidin and immunostaining for PKC-δ. **o**, Stimulus–response (I/O) curves for neurons based on electrophysiological profile (late-firing, $n = 22$; regular spiking, $n = 14$) or PKC-δ expression (PKC-δ$^+$, $n = 14$; PKC-δ$^-$, $n = 12$) in CEl. See also Supplementary Tables 2–4. Values are means ± s.e.m.

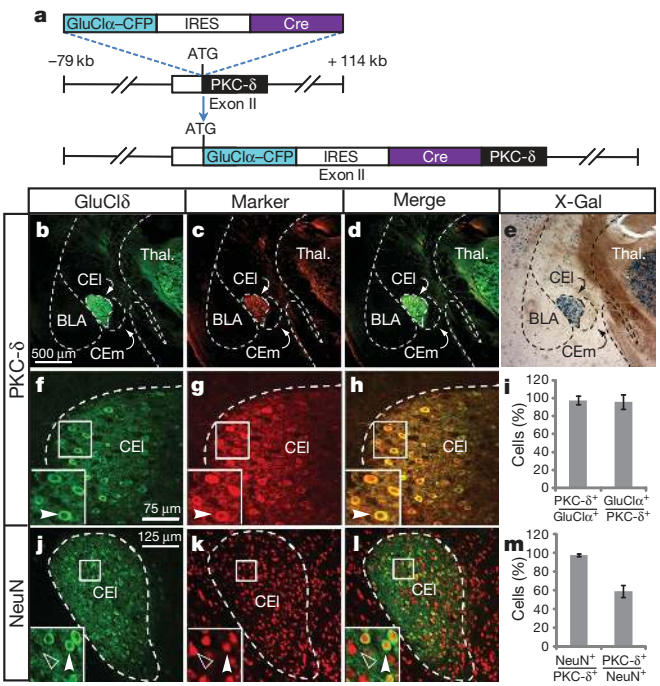

Figure 2 | Transgenic targeting of PKC-δ$^+$ neurons. **a**, Design of PKC-δ::GluClα−CFP-iresCre BAC transgene. kb, kilobases. **b–d**, **f–h**, **j–l**, Expression of transgene visualized by double-label immunofluorescent labelling for GFP and the indicated markers. **i**, **m**, Quantification of **f–h** and **j–l**, respectively. Values are means ± s.e.m. ($n = 3$). **e**, Staining of PKC-δ::GluClα-iresCre; Rosa::loxP-STOP-loxP-lacZ mice with 5-bromo-4-chloro-3-indolyl-β-D-galactoside (X-Gal) reveals β-galactosidase expression (blue) in correct locations. Scale bar in **b** applies to **c–h** and **j–l**.

PKC-δ$^+$ (Fig. 3m–o, white arrowhead in inset); the remainder were PKC-δ$^-$.

Freezing is controlled by projections from CEm to the peri-aqueductal grey (PAG)[32–34], but CEm contains multiple neuronal subpopulations with different connectivities[34]. To determine whether PKC-δ$^+$ neurons make inhibitory synapses onto PAG-projecting CEm output neurons, we combined whole-cell patch clamp recording of retrogradely labelled CEm output neurons, with Cre-dependent optogenetic activation[35] of PKC-δ$^+$ neurons (Fig. 3p, q), in acute amygdala slices. Selective expression of channelrhodopsin-2 (ChR2)[36] in PKC-δ$^+$ neurons was achieved by injecting a Cre-dependent AAV encoding yellow fluorescent protein (YFP)-tagged ChR2 (ref. 37) into the CEl of PKC-δ:GluClα-ires-Cre transgenic mice (Supplementary Fig. 9a). Whole-cell patch-clamp recordings from ChR2-expressing PKC-δ$^+$ neurons (identified using native fluorescence for YFP (ChR2) and CFP (GluClα; Supplementary Fig. 9b)) confirmed that spiking could be induced with about 90% efficiency with 473-nm light flashes at 15 Hz (Supplementary Fig. 9g). Retrograde labelling of CEm projection neurons in the same animals was achieved by injection of Alexa-555-conjugated CTB into the PAG (Fig. 3p), permitting their prospective identification by native fluorescence (Fig. 3q, arrowhead).

In slices prepared from doubly injected animals, optogenetic activation of CEl PKC-δ$^+$ neurons elicited robust, picrotoxin-sensitive inhibitory postsynaptic currents (IPSCs) in CEm output neurons (success rate 100%) (Fig. 3r, s; IPSC amplitude 18.3 ± 2.3 pA, $n = 6$ cells) with an average latency of 3.7 ± 0.2 ms (range 2–5 ms, $n = 30$) and a mean temporal jitter of 0.83 ± 0.16 ms ($n = 6$), consistent with monosynaptic transmission[38]. It also suppressed current-injection-evoked action potentials in CEm output neurons (Fig. 3t, v) in a picrotoxin-sensitive manner (Fig. 3u, w). Thus, CEl PKC-δ$^+$ neurons make inhibitory connections onto PAG-projecting CEm output neurons.

Activation of ChR2-expressing PKC-δ$^+$ neurons by light also evoked monosynaptic IPSCs and suppressed current-injection-evoked action potential firing in CEl PKC-δ$^-$ neurons (identified by the absence of CFP fluorescence), in a picrotoxin-sensitive manner (Fig. 4a–g). PKC-δ$^+$ neurons therefore also make local inhibitory connections within CEl onto PKC-δ$^-$ neurons.

To determine whether, conversely, PKC-δ$^+$ neurons receive inhibitory input from PKC-δ$^-$ neurons, we employed a cell-specific modification of a virally based monosynaptic retrograde tracing method[39]. PKC-δ::GluClα-ires-Cre transgenic mice were first injected with a Cre-dependent AAV encoding both the avian sarcoma/leukosis virus subtype A receptor TVA, and a complementing RV-G protein deleted from the rabies virus strain RV$^{\Delta G}$ (Fig. 4h, left)[40]. Three weeks later, animals were injected in the same site with Env(A)-pseudotyped RV$^{\Delta G}$ virus expressing the red fluorescent protein mCherry (Fig. 4h, right; see Methods). Because Env(A) directs infection exclusively to TVA-expressing cells[39], this manipulation yields expression of mCherry in CEl PKC-δ$^+$ neurons in transgenic mice (Fig. 4m–p; inset, open arrowheads) but not in wild-type mice (Fig. 4i, j). Expression of rabies B19 glycoprotein by AAV-infected PKC-δ$^+$ neurons permits the trans-synaptic spread of the RV$^{\Delta G}$ virus to input neurons, but no further spread occurs[39]. Monosynaptic retrograde labelling of PKC-δ$^-$ neurons occurred extensively in CEl (Fig. 4m, n, p; inset, filled arrowheads), and most labelled neurons were GABAergic (Fig. 4q–t; inset, arrowhead). These data suggest that PKC-δ$^+$ neurons receive inhibitory input from PKC-δ$^-$ neurons.

PKC-δ$^+$ neurons correspond to CEl$_{off}$ units

Single-unit recording experiments in freely behaving mice have identified two types of CEl units with opposite responses to the CS[16]: units

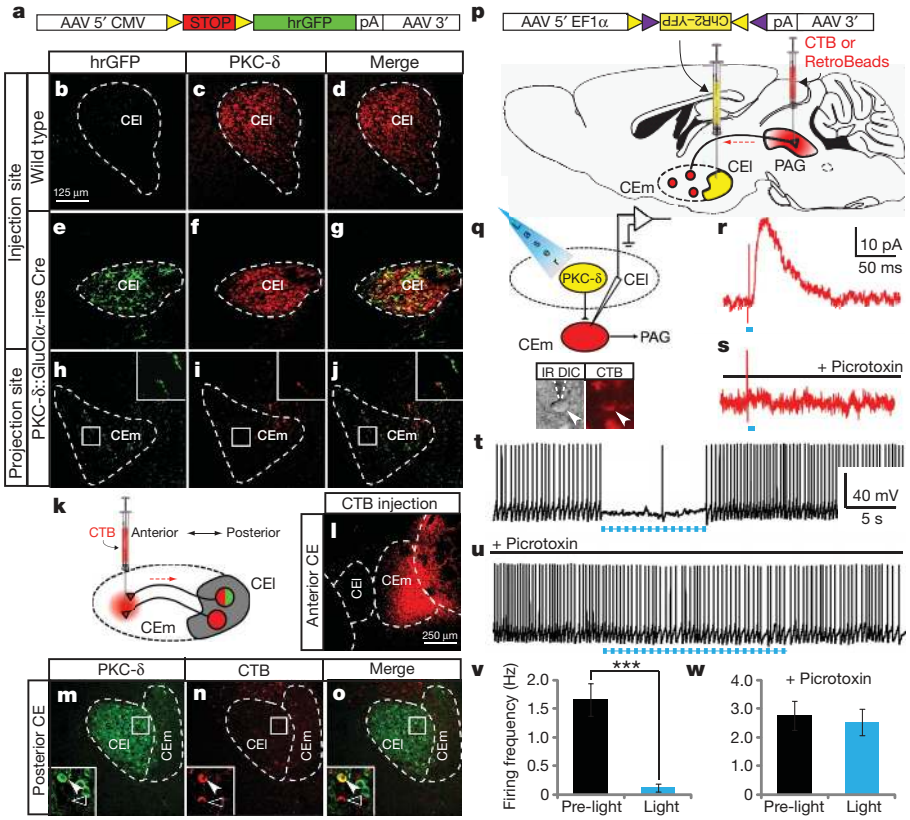

Figure 3 | CEl PKC-δ$^+$ neurons directly inhibit CEm output neurons. **a**–**j**, Anterograde axonal tracing with the use of Cre-dependent hrGFP AAV[31]. **k**–**o**, Retrograde tracing from CEm using red fluorescent CTB. **p**–**w**, Optogenetic activation of CEl PKC-δ$^+$ neurons inhibits PAG-projecting neurons in CEm. **p**, Diagram illustrating double-injection/slice-recording experiments. **q**, CTB$^+$ CEm cell (CTB, arrowhead) with patch electrode (infrared differential interference contrast (IR DIC), dashed lines) is illustrated. **r**–**v**, Whole-cell voltage-clamp ($V_{hold} = -40$ mV) (**r**, **s**) and current-clamp (**t**–**v**) recordings from a back-labelled CEm neuron. **r**, **s**, IPSC triggered by a 2-ms 473-nm laser pulse, with (**s**) or without (**r**) 100 μM picrotoxin. **t**–**v**, Suppression of depolarizing current-injection-evoked spiking by 473-nm laser pulses (2 ms, 15 Hz), with (**u**) or without (**t**) 100 μM picrotoxin. **v**, **w**, Quantification of data in **t** ($n = 5$ cells; asterisk, $P < 0.001$, *t*-test) and **v** ($n = 3$ cells; $P = 0.75$, *t*-test), respectively. Values are means ± s.e.m.

activated by the tone ('CEl$_{on}$' cells), and units inhibited by it ('CEl$_{off}$' cells) (Fig. 5i–l). We wished to determine whether PKC-δ$^+$ neurons correspond to either of these classes of unit. Because the *in vivo* recordings employed extracellular electrodes[16], the cells could not be filled for antibody staining. We therefore examined the effect of reversibly silencing PKC-δ$^+$ neurons on the activity of CEl$_{on}$ and CEl$_{off}$ units, using a mammalian codon-optimized form[41] of the ivermectin-sensitive chloride channel GluCl from *C. elegans*[14,15], mutated to eliminate glutamate sensitivity[27]. Functional expression of this ionotropic receptor requires two subunits, namely GluClα and GluClβ. To restrict the expression of GluClαβ to CEl PKC-δ$^+$ neurons, we employed an intersectional strategy in which GluClα–CFP was expressed transgenically in all PKC-δ$^+$ neurons (Fig. 2b), whereas GluClβ–YFP[25] was expressed in CEl from an AAV vector by stereotaxic injection (Fig. 5a and Supplementary Fig. 2a–e).

We first confirmed silencing of PKC-δ$^+$ neurons by using ivermectin/GluCl in acute amygdala slices from the mice with intersectional GluClαβ expression. Neurons expressing GluClα and/or GluClβ could be prospectively identified by native CFP and YFP fluorescence, respectively (Fig. 5c–e). Bath application of ivermectin decreased the input resistance of cells expressing GluClαβ, but not that of cells expressing either GluClα or GluClβ, from 337 ± 41 to 277 ± 36 MΩ ($n = 4$, $P < 0.04$, paired *t*-test). Ivermectin also significantly suppressed current-injection-evoked spiking in neurons expressing both subunits (Fig. 5c–h), as well as subthreshold excitatory postsynaptic potentials evoked by stimulation of the lateral nucleus with a bipolar electrode (Supplementary Fig. 3; this bipolar stimulation did not evoke spiking of PKC-δ$^+$ neurons in our slice preparation).

We next examined the effect of silencing PKC-δ$^+$ neurons on CEl$_{on}$ and CEl$_{off}$ unit activity[16], in PKC-δ::GluClα-ires-Cre transgenic mice previously injected in CEl with the AAV::GluClβ virus. CEl$_{on}$ and CEl$_{off}$ units were first identified by CS presentation in conditioned animals, before administration of ivermectin. The spontaneous spiking activity of these units was subsequently measured before, and 3–5 days after, administration of ivermectin. The tonic activity of CEl$_{off}$ units was strongly suppressed after treatment with ivermectin, whereas that of CEl$_{on}$ units was unaffected (Fig. 5m, n). This effect of ivermectin was reversed within 48 h after treatment (Fig. 5m), and was not observed in ivermectin-treated uninjected transgenic animals or in virally injected animals not treated with ivermectin (Fig. 5n). Silencing of PKC-δ$^+$ neurons with ivermectin/GluCl also increased CEm unit activity (Fig. 5m, n, red symbols), which is consistent with our observation that PKC-δ$^+$ CEl neurons inhibit CEm output neurons (Fig. 3q–w). The simplest interpretation of these data is that CEl$_{off}$ units are PKC-δ$^+$ neurons, although this does not necessarily imply the converse.

Behavioural effect of silencing CEl PKC-δ$^+$ neurons

Finally, we tested the effect of suppressing PKC-δ$^+$ neuronal activity on fear conditioning (see Methods). We initially investigated the effect of silencing during both training and testing, analogous to a pre-training lesion. Although ivermectin at the dose used (10 mg kg^{-1}) did not significantly affect freezing in wild-type animals (Supplementary Fig. 4a), to avoid potential interactions between treatment with ivermectin and viral infection, in most experiments we also treated single subunit-expressing control animals (transgenic or wild-type animals injected

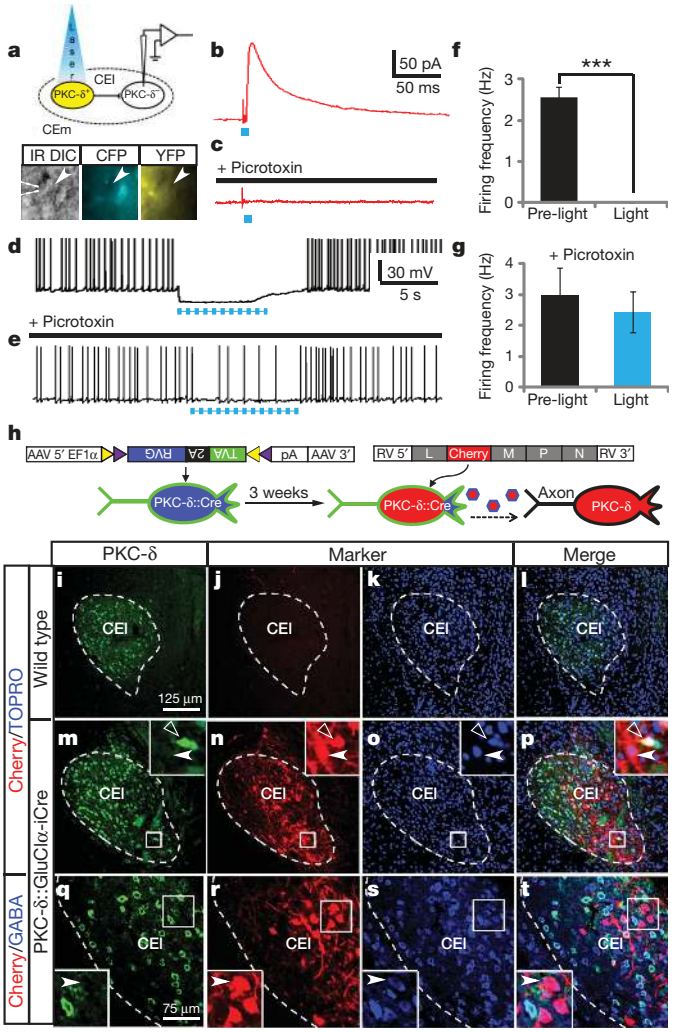

Figure 4 | PKC-δ$^+$ and PKC-δ$^-$ make reciprocal inhibitory connections in CEl. **a**, Diagram and micrograph from slice preparation. Arrowhead indicates PKC-δ (CFP)$^-$, ChR2 (YFP)$^-$ recorded cell in CEl. **b**–**e**, Whole-cell voltage-clamp ($V_{hold} = -40$ mV) (**b**, **c**) and current-clamp (**d**, **e**) recordings from a PKC-δ$^-$ CEl neuron showing light-triggered IPSCs (**b**), picrotoxin-sensitive IPSCs (**c**) or picrotoxin-sensitive (**e**) suppression of depolarizing current-injection-evoked spiking (**d**) by ChR2 activation (blue dots; 2 ms, 15 Hz). **f**, Quantification of data in **d** ($n = 5$ cells; three asterisks, $P < 0.001$, *t*-test). **g**, Quantification of data in **e** ($n = 3$ cells; $P = 0.66$, *t*-test). **h**, Diagram illustrating cell-specific rabies virus infection. **i**–**p**, Immunostaining for PKC-δ (**i**, **m**), intrinsic mCherry fluorescence (**j**, **n**) and nuclear staining with TOPRO-3 (**k**, **o**) 3 days after injection of transgenic (**m**–**p**) and wild-type (**i**–**l**) mice with RV$^{\Delta G}$. Primary infected PKC-δ$^+$ neurons (insets in **m** and **n**, open arrowheads) and retrogradely labelled PKC-δ$^-$ cells (insets in **m** and **n**, filled arrowheads) are indicated. **q**–**t**, Triple labelling for PKC-δ (**q**), GABA (**s**) and mCherry (**r**). mCherry-labelled PKC-δ$^-$ cells are GABAergic (inset, arrowhead). Values are means ± s.e.m.

with GluClα or GluClβ virus, respectively) with ivermectin. These control groups were not significantly different from each other (Supplementary Fig. 4b) and were pooled for statistical analysis.

In some experiments (five to eight animals per group), when we used a high-titre (10^{13} ml^{-1}) preparation of AAV2:GluClβ (ref. 14), a significantly higher level of freezing was observed in experimental animals than in controls; however, in other experiments with different virus preparations, no difference between groups was detected (Supplementary Note 1). Quantitative histological analysis (Supplementary Fig. 10) revealed considerable variation in the level and bilaterality of GluClβ–YFP expression among individual animals (Supplementary Fig. 5a–c). We therefore pooled data from multiple experiments (total $n = 54$ animals/group) for statistical analysis. A randomized-block analysis of variance (ANOVA)[42] with six experimental and six control subjects assigned to each of nine blocks based on infection rate (total $n = 108$; Supplementary Table 5 and Supplementary Fig. 5d–f) indicated a significant block × group interaction during both the CS presentation ($F_{(8,90)} = 2.298$, $P < 0.05$ by post-hoc Bonferroni *t*-test) and post-CS periods ($F_{(8,90)} = 2.459$, $P < 0.05$) but not during the baseline period ($F_{(8,90)} = 1.41$, $P = 0.205$). Freezing was significantly higher in the experimental group only in the block with the highest infection rate (Table 1, Supplementary Table 5 and Supplementary Fig. 5e, f). Freezing in the experimental group was also significantly higher than in controls (including GluClαβ animals tested without ivermectin; $n = 6$) among animals expressing GluClβ bilaterally in the central nucleus at a level above the median infection rate (Supplementary Fig. 7). There was no significant decrease in baseline locomotor activity or in the activity burst produced by the first presentation of the unconditioned stimulus during training (Supplementary Fig. 8) in experimental animals, indicating that the increased freezing was not a consequence of either decreased locomotor activity or increased sensitivity to the unconditioned stimulus[13]. Freezing levels during the pre-training and pre-test baseline were unaffected by ivermectin in experimental animals (Supplementary Table 5, Supplementary Figs 5 and 7, and data not shown).

Discussion

We have used genetically based methods to investigate the functional connectivity of a subpopulation of CEl GABAergic neurons identified by the expression of PKC-δ. Our data suggest that these neurons participate in a recurrent inhibitory circuit within CEl that inhibits CEm output to brainstem centres that control freezing, consistent with earlier suggestions[9,12]. In the accompanying paper[16] two populations of CEl units are identified *in vivo* with opposite responses to the CS. The data presented here strongly suggest that CEl$_{off}$ units are PKC-δ$^+$ neurons, linking molecular and physiological identity. Because PKC-δ$^+$ neurons pre-exist in untrained animals, this linkage suggests that CEl$_{off}$ and CEl$_{on}$ units, which are robustly identifiable after conditioning (Fig. 5k, l), arise through plasticity-dependent changes in deterministic CEl subpopulations rather than by stochastic selection from a population of initially homogeneous cells.

The link between PKC-δ$^+$ neurons and CEl$_{off}$ units is also consistent with complementary connectivity data in the two studies. For example, it has been shown that *in vivo* the activity of CEl$_{off}$ units is inversely correlated with the activity of CEl$_{on}$ units, suggesting reciprocal inhibition[16]. Our channelrhodopsin-assisted circuit mapping[38] and cell-specific

Table 1 | Behavioural effect of silencing PKC-δ$^+$ neurons in CEl

Group (block 9)	Infection rate (%)	Baseline freezing (%)	CS freezing (%)	Post-CS freezing (%)
Control (GluClα or GluClβ + ivermectin)	40.0 ± 0.8	5.8 ± 2.2	49.4 ± 10.4	19.2 ± 6.0
Experimental (GluClαβ + ivermectin)	40.6 ± 3.5	2.6 ± 1.5 (n.s.)	91.1 ± 4.7 ($P < 0.05$)	75.3 ± 8.4 ($P < 0.001$)

The data are derived from the randomized-block ANOVA in Supplementary Table 5 (total $n = 108$; six experimental and six control animals assigned to each of nine blocks), and illustrate the block with the highest level of viral infection in CEl (infection rate: the percentage of PKC-δ$^+$ cells expressing GluClβ–YFP; see Supplementary Fig. 10). The control group was pooled (Supplementary Fig. 4b) single-subunit-expressing mice (GluClα or GluClβ alone) treated with ivermectin. Values are means ± s.e.m.; n.s., not significantly different. *P* values are from a post-hoc Bonferroni *t*-test. A significant linear component to the block × group interaction indicated that the difference between groups tended to increase with infection rate ($F_{(1,90)} = 22.98$, $P < 0.0001$ for CS; $F_{(1,90)} = 8.85$, $P < 0.006$ for post-CS). See also Supplementary Table 5 and Supplementary Fig. 5. Control GluClαβ-expressing mice not treated with ivermectin were significantly different from the experimental group among animals showing bilateral AAV infection above the median rate ($n = 6$–21; Supplementary Fig. 7).

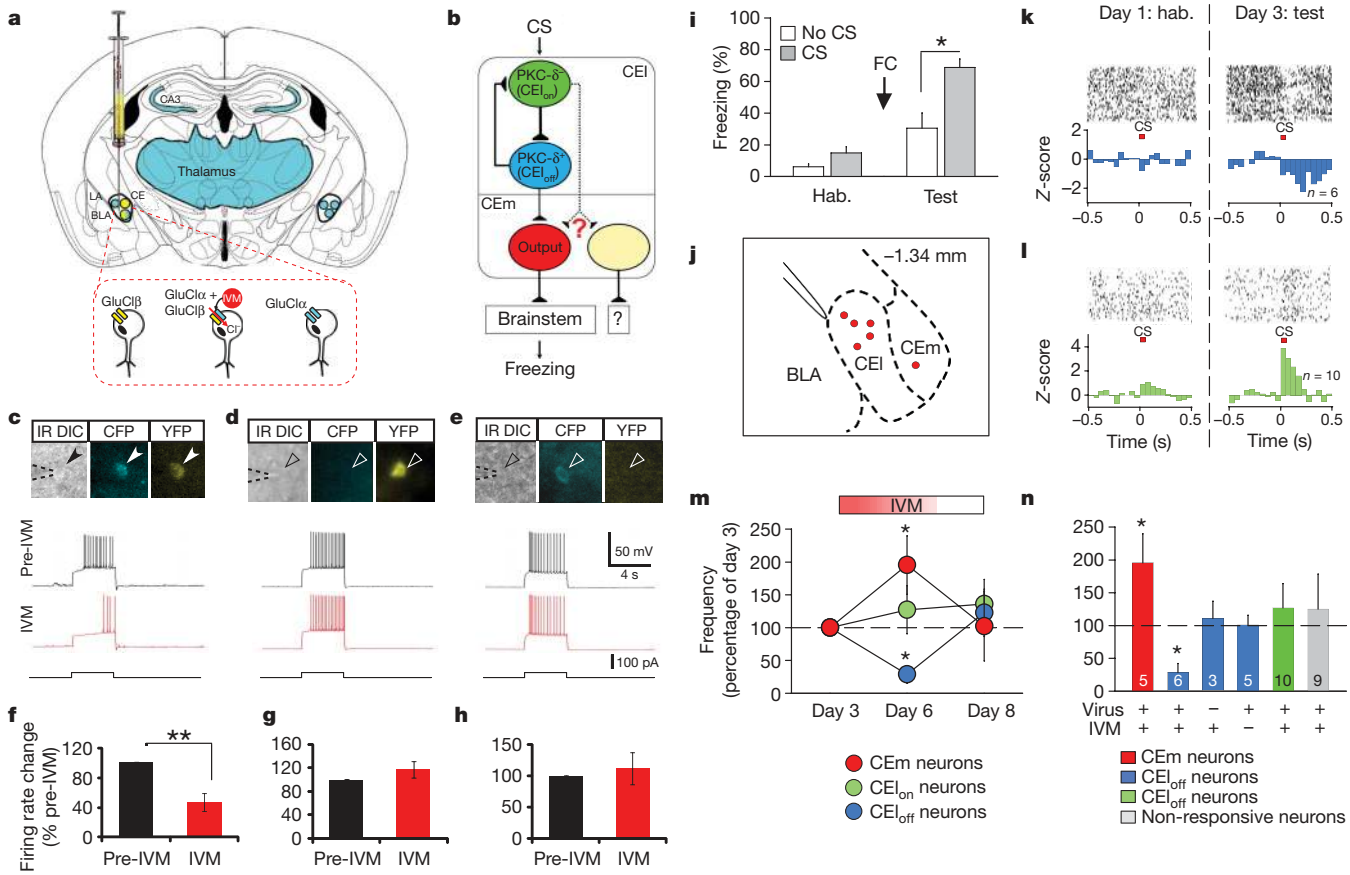

Figure 5 | CEl$_{off}$ neurons are PKC-δ$^+$. **a**, Selective expression of GluClαβ in CEl PKC-δ$^+$ neurons. Yellow, AAV::GluClβ–YFP; blue, PKC-δ::GluClα–CFP transgene. **b**, Inhibitory connections in CE[16]. **c**–**e**, PKC-δ$^+$ cells expressing GluClαβ (**c**), GluClβ–YFP (**d**) or GluClα–CFP (**e**). Upper and middle traces, spiking before and after ivermectin (IVM) (20 nM), respectively; bottom trace, current injection. **f**–**h**, Quantification of **c**–**e** (**f**, $n = 4$ cells, $P = 0.005$; **g**, $n = 5$ cells, $P = 0.73$; **h**, $n = 4$ cells, $P = 0.66$; paired t-tests). **i**–**n**, Silencing PKC-δ$^+$ neurons during chronic *in vivo* recording. **i**, Behavioural data for recorded mice. Hab., habituation; FC, fear conditioning ($n = 5$). **j**, Coronal diagram showing recording sites. BLA, basolateral amygdala. **k**, **l**, Representative raster plots (upper) and normalized population peristimulus time histograms (lower) of CEl$_{off}$ (**k**; lower, $n = 6$ neurons, three mice) and CEl$_{on}$ neurons (**l**; lower, $n = 10$ neurons, four mice) showing CS-evoked changes ($P < 0.05$). For unit isolation see Supplementary Fig. 11. **m**, Tonic activity of CEl$_{off}$ (one-way ANOVA ($F_{(2,15)} = 4.845$, $P = 0.024$) with post-hoc Bonferroni t-test (asterisk, $P < 0.05$)), but not of CEl$_{on}$ neurons (one-way ANOVA ($F_{(2,27)} = 0.391$, $P = 0.680$)), is significantly (day 6) and reversibly (day 8) decreased by ivermectin, whereas CEm activity is increased ($n = 5$ units, one mouse; one-way Kruskal–Wallis ANOVA ($H = 7.487$, $P = 0.024$) with post-hoc Tukey's Honestly Significant Difference (asterisk, $P < 0.05$)). **n**, Specificity controls for **m**. Asterisk, $P < 0.05$ (paired t-tests, treatment versus pre-treatment values)). Ivermectin injection without virus ($n = 3$; $P = 0.765$); AAV2::GluClβ virus without ivermectin ($n = 5$; $P = 0.940$). CEl$_{on}$ neurons ($n = 10$; $P = 0.497$); CS-non-responsive neurons ($n = 9$; $P = 0.644$). Error bars show s.e.m.

monosynaptic retrograde viral tracing[39] data directly demonstrate mutual inhibitory connections between PKC-δ$^+$ and PKC-δ$^-$ neurons in CEl. It has also been shown that exposure to CS both inhibits CEl$_{off}$ unit spiking and increases CEm unit activity[16], with a short latency implying an inhibitory connection. Our data directly demonstrate inhibitory synapses from CEl PKC-δ$^+$ neurons onto brainstem-projecting CEm output neurons, and indicate that silencing the former increases the tonic activity of the latter *in vivo*. Thus, our direct mapping of PKC-δ$^+$ synaptic connectivity in amygdala slices is consistent with inferences of CEl$_{off}$ unit connectivity based on correlative *in vivo* recordings (Fig. 5b).

Consistent with these electrophysiological and connectional data, genetic silencing of PKC-δ$^+$ neurons yielded a statistically significant enhancement of conditional freezing (during both the CS-on and post-CS periods) among those animals with the highest level of AAV::GluClβ infection in CEl. Nevertheless, these behavioural results should be interpreted with caution, given the variability in results between individual experiments (see Supplementary Note 1). Furthermore, although treatment with ivermectin caused a decrease in CEl$_{off}$ tonic spiking activity in GluClαβ-expressing animals, how this effect influences CS-evoked freezing, which is correlated with phasic CS response in CEl$_{off}$ unit activity[16], is not yet clear.

Although the CEl circuitry defined here and in ref. 16 is remarkably consistent, the behavioural results in the two studies differ in some respects. For example, muscimol injection into CEl evoked freezing in unconditioned animals[16], whereas selective silencing of PKC-δ$^+$ neurons with ivermectin/GluCl did not. Furthermore, transient inhibition of CEl during training with muscimol attenuated fear conditioning[16], whereas chronic silencing of PKC-δ$^+$ neurons during both training and testing did not. We have not yet examined the behavioural effects of silencing PKC-δ$^+$ neurons during training compared with testing, and this will be a significant question for future studies. Differences between the consequences of the inhibition of CEl by muscimol and those arising from the silencing of CEl PKC-δ$^+$ neurons by ivermectin/GluCl may reflect differences in the cellular specificity, efficiency or time course of the two types of manipulation (Supplementary Note 2).

The CEl/CEm microcircuit revealed by these companion studies has properties worthy of further investigation. For example, the mutual inhibitory connections between CEl$_{off}$ and CEl$_{on}$ units could provide a positive feedback loop to amplify CS-evoked activity in CEl$_{on}$ units (Fig. 5b)[43]. These antagonistic connections could also potentially encode different states, through stable imbalances in tonic activity[16] or different oscillatory regimes, that could influence the learning and/or expression of conditioned fear. A currently unresolved paradox is

why, if CEl_{on} units (like CEl_{off} units) send inhibitory projections to CEm[16], the activation of CEl_{on} units by the CS results in increased rather than decreased activity of CEm output neurons (see Supplementary Note 3). Resolution of this paradox will require determining whether these two CEl populations target the same or different classes of CEm neuron[34], and the relative strength of these connections. Genetically based synaptic tracing and functional manipulations of CEl_{on} units should clarify this issue, and should also provide direct tests of their causal role in conditioned freezing and other emotional behaviours. The ability to identify and selectively manipulate PKC-δ^+ and other molecularly defined CEl subpopulations prospectively[44,45] should also open the way to investigating their roles in animal models of phobic or anxiety disorders, and in the mechanism of action of drugs used to treat such disorders[46].

METHODS SUMMARY

Histochemical methods. Single-colour and double-label fluorescence *in situ* hybridizations were performed on fresh frozen sections, using RNA probes labelled with digoxigenin (Roche) and with 2,4-dinitrophenol (PerkinElmer). Immunofluorescence was performed on cryosections of tissue perfused with 4% paraformaldehyde, following standard protocols.

Generation of PKC-δ::GluClα-ires-Cre transgenic mice. A GluClα-ires-Cre cassette was inserted into PKC-δ BAC clone RP23-283B12 (CHORI). The modified BAC was injected into FVB mouse embryos (GENSAT). Transgenic founders were backcrossed ($n > 5$) to C57Bl6/N. These mice are available through GENSAT[26].

Pharmacogenetic silencing *in vitro* and *in vivo*. PKC-δ::GluClα-ires-Cre transgenic or wild-type mice were injected with about 10^9 particles of AAV::GluClβ (or, in control experiments, AAV::GluClα) into the central amygdala and allowed to recover for 4 weeks. For fear conditioning experiments, mice were habituated and then injected with ivermectin (10 mg kg^{-1}; Phoenix) on day 1. On day 2, animals received tone/foot-shock pairings in context A (Coulbourn, Med Associates). On day 3, (and for *in vivo* recordings also on days 6 and 8), animals were placed in context B and freezing was scored before (baseline), during and after CS presentations. For *in vitro* recordings, acute brain slices were prepared and superfused with 20 nM ivermectin in artificial cerebrospinal fluid to induce pharmacogenetic silencing. Single-unit recordings were performed in freely behaving animals as described[16].

Optogenetic circuit dissection. PKC-δ::GluClα-ires-Cre transgenic mice were injected with 10^9 particles of Cre-dependent ChR2 AAV into the central amygdala, and (in some animals) CTB into the PAG for retrograde labelling. Four weeks later, neurons were stimulated with light, in acute brain slices, through a 200-μm optical fibre (Thorlabs) emitting 5–10 mW of 473-nm laser light (Crystalaser).

Virus based trans-synaptic tracing. PKC-δ::GluClα-ires-Cre transgenic mice were injected sequentially into the central amygdala with 10^4 particles of AAV encoding Cre-dependent TVA and rabies B19 glycoprotein. Three weeks later, animals were injected in the same site with 10^5 particles of $RV^{\Delta G}$ rabies virus pseudotyped with EnvA, and analysed one week later. All animal experiments were conducted under protocols approved by the Caltech Institutional Animal Care and Use Committee (IACUC) and the Salk Institute Biosafety Committee.

Full Methods and any associated references are available in the online version of the paper at www.nature.com/nature.

Received 23 February; accepted 6 October 2010.

1. Davis, M., Walker, D. L. & Myers, K. M. Role of the amygdala in fear extinction measured with potentiated startle. *Ann. NY Acad. Sci.* **985,** 218–232 (2003).
2. LeDoux, J. E. Emotion circuits in the brain. *Annu. Rev. Neurosci.* **23,** 155–184 (2000).
3. Paré, D., Quirk, G. J. & LeDoux, J. E. New vistas on amygdala networks in conditioned fear. *J. Neurophysiol.* **92,** 1–9 (2004).
4. Pitkänen, A., Savander, V. & LeDoux, J. E. Organization of intra-amygdaloid circuitries in the rat: an emerging framework for understanding functions of the amygdala. *Trends Neurosci.* **20,** 517–523 (1997).
5. Maren, S. & Quirk, G. J. Neuronal signalling of fear memory. *Nature Rev. Neurosci.* **5,** 844–852 (2004).
6. Medina, J. F., Repa, J. C., Mauk, M. D. & LeDoux, J. E. Parallels between cerebellum- and amygdala-dependent conditioning. *Nature Rev. Neurosci.* **3,** 122–131 (2002).
7. Cassell, M. D., Freedman, L. J. & Shi, C. The intrinsic organization of the central extended amygdala. *Ann. NY Acad. Sci.* **877,** 217–241 (1999).
8. Cassell, M. D., Gray, T. S. & Kiss, J. Z. Neuronal architecture in the rat central nucleus of the amygdala: a cytological, hodological, and immunocytochemical study. *J. Comp. Neurol.* **246,** 478–499 (1986).
9. Day, H. E. W., Curran, E. J., Watson, S. J. & Akil, H. Distinct neurochemical populations in the rat central nucleus of the amygdala and bed nucleus of the stria terminalis: evidence for their selective activation by interleukin-1β. *J. Comp. Neurol.* **413,** 113–128 (1999).
10. Marchant, N. J., Densmore, V. S. & Osborne, P. B. Coexpression of prodynorphin and corticotrophin-releasing hormone in the rat central amygdala: evidence of two distinct endogenous opioid systems in the lateral division. *J. Comp. Neurol.* **504,** 702–715 (2007).
11. Ehrlich, I. *et al.* Amygdala inhibitory circuits and the control of fear memory. *Neuron* **62,** 757–771 (2009).
12. Huber, D., Veinante, P. & Stoop, R. Vasopressin and oxytocin excite distinct neuronal populations in the central amygdala. *Science* **308,** 245–248 (2005).
13. Wilensky, A. E., Schafe, G. E., Kristensen, M. P. & LeDoux, J. E. Rethinking the fear circuit: the central nucleus of the amygdala is required for the acquisition, consolidation, and expression of Pavlovian fear conditioning. *J. Neurosci.* **26,** 12387–12396 (2006).
14. Lerchner, W. *et al.* Reversible silencing of neuronal excitability in behaving mice by a genetically targeted, ivermectin-gated Cl^- channel. *Neuron* **54,** 35–49 (2007).
15. Slimko, E. M., McKinney, S., Anderson, D. J., Davidson, N. & Lester, H. A. Selective electrical silencing of mammalian neurons *in vitro* by the use of invertebrate ligand-gated chloride channels. *J. Neurosci.* **22,** 7373–7379 (2002).
16. Ciocchi, S. *et al.* Encoding of conditioned fear in central amygdala inhibitory circuits. *Nature* doi:10.1038/nature09559 (this issue).
17. Day, H. E., Nebel, S., Sasse, S. & Campeau, S. Inhibition of the central extended amygdala by loud noise and restraint stress. *Eur. J. Neurosci.* **21,** 441–454 (2005).
18. Zirlinger, M. & Anderson, D. Molecular dissection of the amygdala and its relevance to autism. *Genes Brain Behav.* **2,** 282–294 (2003).
19. Zirlinger, M., Kreiman, G. & Anderson, D. J. Amygdala-enriched genes identified by microarray technology are restricted to specific amygdaloid subnuclei. *Proc. Natl Acad. Sci. USA* **98,** 5270–5275 (2001).
20. Callaway, E. M. A molecular and genetic arsenal for systems neuroscience. *Trends Neurosci.* **28,** 196–201 (2005).
21. Luo, L., Callaway, E. M. & Svoboda, K. Genetic dissection of neural circuits. *Neuron* **57,** 634–660 (2008).
22. Zhang, F., Aravanis, A. M., Adamantidis, A., de Lecea, L. & Deisseroth, K. Circuit-breakers: optical technologies for probing neural signals and systems. *Nature Rev. Neurosci.* **8,** 577–581 (2007).
23. Chieng, B. C., Christie, M. J. & Osborne, P. B. Characterization of neurons in the rat central nucleus of the amygdala: cellular physiology, morphology, and opioid sensitivity. *J. Comp. Neurol.* **497,** 910–927 (2006).
24. Schiess, M. C., Callahan, P. M. & Zheng, H. Characterization of the electrophysiological and morphological properties of rat central amygdala neurons *in vitro*. *J. Neurosci. Res.* **58,** 663–673 (1999).
25. Lopez de Armentia, M. & Sah, P. Firing properties and connectivity of neurons in the rat lateral central nucleus of the amygdala. *J. Neurophysiol.* **92,** 1285–1294 (2004).
26. Gong, S. *et al.* A gene expression atlas of the central nervous system based on bacterial artificial chromosomes. *Nature* **425,** 917–925 (2003).
27. Li, P., Slimko, E. M. & Lester, H. A. Selective elimination of glutamate activation and introduction of fluorescent proteins into a *Caenorhabditis elegans* chloride channel. *FEBS Lett.* **528,** 77–82 (2002).
28. Wagstaff, M. J. *et al.* Gene transfer using a disabled herpes virus vector containing the EMCV IRES allows multiple gene expression *in vitro* and *in vivo*. *Gene Ther.* **5,** 1566–1570 (1998).
29. Veinante, P. & Freund-Mercier, M. J. Branching patterns of central amygdaloid nucleus afferents in the rat: single axon reconstructions. *Ann. NY Acad. Sci.* **985,** 552–553 (2003).
30. Sun, N., Yi, H. & Cassell, M. D. Evidence for a GABAergic interface between cortical afferents and brainstem projection neurons in the rat central extended amygdala. *J. Comp. Neurol.* **340,** 43–64 (1994).
31. Gautron, L., Lazarus, M., Scott, M. M., Saper, C. B. & Elmquist, J. K. Identifying the efferent projections of leptin-responsive neurons in the dorsomedial hypothalamus using a novel conditional tracing approach. *J. Comp. Neurol.* **518,** 2090–2108 (2010).
32. De Oca, B. M., De Cola, J. P., Maren, S. & Fanselow, M. S. Distinct regions of the periaqueductal gray are involved in the acquisition and expression of defensive responses. *J. Neurosci.* **18,** 3426–3432 (1998).
33. Kim, J. J., Rison, R. A. & Fanselow, M. S. Effects of amygdala, hippocampus, and periaqueductal grady lesions on short- and long-term contextual fear. *Behav. Neurosci.* **107,** 1093–1098 (1993).
34. LeDoux, J. E., Iwata, J., Cicchetti, P. & Reis, D. J. Different projections of the central amygdaloid nucleus mediate autonomic and behavioral correlates of conditioned fear. *J. Neurosci.* **8,** 2517–2529 (1988).
35. Kravitz, A. V. *et al.* Regulation of parkinsonian motor behaviours by optogenetic control of basal ganglia circuitry. *Nature* **466,** 622–626 (2010).
36. Zhang, F. *et al.* Multimodal fast optical interrogation of neural circuitry. *Nature* **446,** 633–639 (2007).
37. Cardin, J. A. *et al.* Targeted optogenetic stimulation and recording of neurons *in vivo* using cell-type-specific expression of Channelrhodopsin-2. *Nature Protocols* **5,** 247–254 (2010).
38. Petreanu, L., Huber, D., Sobczyk, A. & Svoboda, K. Channelrhodopsin-2-assisted circuit mapping of long-range callosal projections. *Nature Neurosci.* **10,** 663–668 (2007).
39. Wickersham, I. R. *et al.* Monosynaptic restriction of transsynaptic tracing from single, genetically targeted neurons. *Neuron* **53,** 639–647 (2007).

40. Wickersham, I. R., Finke, S., Conzelmann, K. K. & Callaway, E. M. Retrograde neuronal tracing with a deletion-mutant rabies virus. *Nature Methods* **4,** 47–49 (2007).
41. Slimko, E. M. & Lester, H. A. Codon optimization of *Caenorhabditis elegans* GluCl ion channel genes for mammalian cells dramatically improves expression levels. *J. Neurosci. Methods* **124,** 75–81 (2003).
42. Edwards, A. L. *Experimental Design in Psychological Research* 4th edn, 249–251 (Holt, Reinhard & Winston, 1972).
43. Wickens, J. R., Arbuthnott, G. W. & Shindou, T. Simulation of GABA function in the basal ganglia: computational models of GABAergic mechanisms in basal ganglia function. *Prog. Brain Res.* **160,** 313–329 (2007).
44. Gozzi, A. *et al.* A neural switch for active and passive fear. *Neuron* **67,** 656–666 (2010).
45. Tsetsenis, T., Ma, X. H., Lo Iacono, L., Beck, S. G. & Gross, C. Suppression of conditioning to ambiguous cues by pharmacogenetic inhibition of the dentate gyrus. *Nature Neurosci.* **10,** 896–902 (2007).
46. Ressler, K. J. & Mayberg, H. S. Targeting abnormal neural circuits in mood and anxiety disorders: from the laboratory to the clinic. *Nature Neurosci.* **10,** 1116–1124 (2007).

Supplementary Information is linked to the online version of the paper at www.nature.com/nature.

Acknowledgements We thank N. Heinz and X. Gong for generating BAC transgenic mice; C. Saper for providing the Cre-dependent hrGFP AAV construct; C. Xiao for training in slice electrophysiology and preliminary experiments; H. Lester for advice on the GluCl system; L. van Tright for performing *in situ* hybridizations; W. Lerchner for providing a CAG-driven GluClβ construct; A. Chang for help with behavioural scoring; M. Martinez for tail genotyping; G. Mosconi for laboratory management; and J. Alex, R. Bayon and R. Sauza for animal care. This work was supported by NIH grant 1 R01 MH085082-01A1 and by funds from the Caltech 'Conscious Mouse' project. W.H. was supported by a fellowship of the Human Frontier Science Program and P.S.K. by the Jane Coffin Childs Memorial Fund for Medical Research. S.C. and A.L. were supported by the Novartis Research Foundation. D.J.A. is an Investigator of the Howard Hughes Medical Institute.

Author Contributions W.H. initiated the project, generated BAC constructs, designed experiments, performed anatomical, viral injections and behavioural experiments, and wrote the manuscript. P.S.K. contributed to experimental design, performed viral injections, behavioural experiments, data analysis and interpretation. H.C. contributed to experimental design and performed viral injections and slice electrophysiology experiments, data analysis and interpretation. S.C. and A.L. designed, performed and interpreted *in vivo* recording experiments (Fig. 5). N.R.W. and E.M.C. performed rabies virus injection experiments. R.P. performed supplementary behavioural experiments and M.S.F. contributed to their interpretation and to statistical analysis. J.B. and H.-W.D. performed supplementary stereotaxic viral injection experiments. K.D. provided Cre-dependent ChR2 constructs and advice. D.J.A. conceived the project, contributed to experimental design and interpretation and wrote the manuscript. P.S.K., H.C. and S.C. contributed equally. All authors discussed the results and commented on the manuscript.

Author Information Reprints and permissions information is available at www.nature.com/reprints. The authors declare no competing financial interests. Readers are welcome to comment on the online version of this article at www.nature.com/nature. Correspondence and requests for materials should be addressed to D.J.A. (wuwei@caltech.edu).

METHODS

Generation of PKC-δ::GluClα-iCre transgenic mice. The PKC-δ::GluClα-iCre targeting construct was assembled in pGEM-T Easy (Promega) by PCR-cloning nucleotides −425 to −1 (+1 corresponding to the PKC-δ start codon, primer set 5′-ACACACCGCGGCGCGCCCTAAAGAGGCAGGAGGCATGTG-3′ and 5′-CCATGATGGAGCCTGGAGTGAG-3′) and +4 to +561 (primer set 5′-TCTCTGCTAGCCCGGGACCCTTCCTGCGCATCTC-3′ and 5-TGTGTG GTCGACTTAATTAAACTAGTGACCTTTCCAGCCATCACGTG-3′) of PKC-δ genomic sequences 5′ and 3′ to the GluClα open reading frame (ORF)[41], using *Ksp*I-blunt/*Mlu*NI and *Nhe*I–*Sal*I restriction sites, respectively. The resulting PKC-δ::GluClα cassette was then cloned into the pLD53 shuttle vector[47]. An additional expression cassette containing the encephalomyocarditis virus internal ribosome entry site (IRES) followed by an ORF coding for Cre-recombinase was cloned into the *Nhe*I site immediately downstream of GluClα. This vector was then used to introduce the GluClα-iCre expression cassette into a BAC clone containing the complete gene encoding PKC-δ (RP23-283B12) by Rec A-mediated homologous recombination in bacteria[47]. Homologous recombination was verified by PCR (5′ arm primer set 5′-AGACCAGGGTAGGAGTCGGTG-3′ and 5′-GATCAGG GAAGCGATGATCAG-3′; 3′ arm primer set 5′-GAGACCAAGACCGAGT GGAA-3′ and 5′-CACAGGTTAGCCATGACCTG-3′) and Southern blotting (5′ arm probe primer set 5′-TGTTCATGGGGTTTCTCACAG-3′ and 5′-ACCG ACTCCTACCCTGGTCAG-3′; 3′ arm probe primer set 5′-AGGTCATGGC TAACCTGTGG-3′ and 5′-GGCAGAGAAGTCAGACTGGG-3′). Transgenic mice were generated by pronuclear injection of CsCl-prepared BAC DNA linearized with P-*Sce*I in FVB embryos[26], which yielded two independent transgenic lines with indistinguishable expression patterns. One of them was backcrossed for more than five generations to C57Bl6/N. Germline transmission and genotyping of transgenic offspring were traced by PCR on genomic tail DNA (primer set 5′-GCTACA TCAAGGCCATCGAC-3′ and 5′-AACTCCAGCAGGACCATGTGATCG-3′). The line is available through GENSAT.

***In situ* hybridizations.** *In situ* hybridization was performed on fresh frozen brain sections 20 µm thick.

Processing of sections, hybridization and probe detection for single colour *in situ* hybridizations were performed with standard protocols[19], with the following specifications: probes were cloned from whole mouse brain cDNA library (Invitrogen; GAD65 primer set 5′-ATCTCCAACATGTATGCCATGCTCATT GCC-3′ and 5′-TTACAAATCTTGTCCGAGGCGTTCGA-3′; corticotropin-releasing hormone primer set 5′-AACGGAGTAAGGGCAGGAATGGAGACA GAG-3′ and 5′-GTTGCTGTGAGCTTGCTGAGCTAACTGCTCTGC-3′; enkephalin primer set 5′-TAGGGTCCAAGCTCTCATTGAGGCACCCGG-3′ and 5′-GCTTCAGAACCGCATAAAGCCCCCGTAT-3′; oxytocin receptor 5′-CTG GCCCACCAGGCCAGCCGCTGGGTGGTG-3′ and 5′-AATCCCCATCTCCT TGGGAATTTTAGGAT-3′) transcribed from linearized templates in pTeasy (Promega) or pCR2.1 (Invitrogen) using Sp6 polymerase (9PIP108; Promega) or T7 polymerase (9PIP207; Promega) and digoxigenin-labelled nucleotide mix (11277073910; Roche), used at a final concentration of 1 µg ml^{-1}, and detected with anti-digoxigenin–horseradish peroxidase, Fab fragments (1-207-733; Roche).

Processing of sections and hybridization for double-label fluorescence *in situ* hybridization were performed as above, with the following specifications: digoxigenin and 2,4-dinitrophenol-UTP (NEL555001; PerkinElmer) probe pairs were used at a final concentration of 1 µg ml^{-1} each. For detection, sections were each blocked first in 20% sheep serum in 0.1 M Tris-HCl pH 7.5, 0.15 M NaCl, 0.05% Tween 20 and NEN-blocking solution (PerkinElmer) for 30 min. Digoxigenin-labelled probe was detected with anti-digoxigenin horseradish peroxidase (Roche) (1:500 dilution, 2 h), biotin-tyramide (1:100 dilution, 8 min, room temperature (20–25 °C); PerkinElmer), Vecta Stain Elite ABC Kit (PK-6100; Vector) and Cy3-Tyramide (Cy3 tyramide NEL704A, 1:50 dilution, 1 h; PerkinElmer). Horseradish peroxidase was inactivated by incubation for 1 h in 3% H_2O_2 in PBS, followed by heat denaturation at 85 °C for 5 min in 10 mM tris(hydroxymethyl) aminomethane, 1 mM EDTA pH 7.5. Sections were blocked again as above and 2,4-dinitrophenol (DNP)-labelled nucleotides were detected with anti-DNP horseradish peroxidase (1:500, 2h), DNP-tyramide, anti-DNP horseradish peroxidase (1:500 dilution, 2 h, all TSA DNP Kit, NEL747A; PerkinElmer) and fluorescein-tyramide (1:100 dilution, NEL701; PerkinElmer). Sections were mounted in Fluoro Gel (17985-10; Electron Microscopy Sciences). All washing steps and incubations were performed in accordance with the respective manufacturers' recommendations. Sections were viewed under a Zeiss Axioscope microscope and a Leica TCS SP confocal microscope.

Immunofluorescent labelling. For immunofluorescent labelling, mice were transcardially perfused with 4% paraformaldehyde in PBS. Brains were removed and cryoprotected for 16 h at 4 °C in 15% sucrose. Cryo-sections 20–30 µm thick were dried in air for 30 min and then rehydrated in PBST (PBS plus 0.1% Triton X-100). In some instances, immunoreactivity was increased by incubating the slides in 10 mM sodium citrate, 0.05% Tween 20 pH 6 for 10 min at 95 °C. Non-specific binding was blocked with 1% BSA in PBST for 30 min. Primary antibodies (mouse anti-PKC-δ (610398; BD Biosciences), guinea-pig anti-dynorphin (GP10110; Neuromics), rabbit anti-GFP (A11122; Invitrogen), rabbit anti-hrGFP (240142; Stratagene), mouse anti-NeuN (MAB377; Chemicon), goat anti-CTB (703; List) diluted 1:300–1:1,000 in blocking solution, were incubated for 16 h at 4 °C. Standard secondary antibodies (Invitrogen) in blocking solution were incubated for 3 h at room temperature. Unbound primary and secondary antibodies were each washed by incubation three times in PBST for 10 min. Sections were mounted in Fluoro Gel (17985-10; Electron Microscopy Sciences) and viewed under a Zeiss Axioscope microscope and a Leica TCS SP confocal microscope.

Animal maintenance. Animals were group housed at 23 °C with *ad libitum* access to food and water in a 13-h day/11-h night cycle, with the day starting at 07:00.

Histological analysis. All histological quantifications (Fig. 2i, m, Supplementary Figs 2e, j, 5, 7 and 10, and Supplementary Tables 1 and 5) are based on at least three coronal sections spaced equidistantly along the rostro-caudal axis of the central amygdala.

The intrinsic fluorescence of GluClα−CFP or GluClβ–YFP can be readily detected in live brain slices (Fig. 4a and 5c–e and Supplementary Fig. 9a, b). In the perfusion-fixed tissue used for all histological analysis, however, the fluorescent signal is substantially weaker. GFP immunofluorescent labelling directed against its CFP or YFP tag was therefore used wherever possible for more accurate results (Fig. 1b–h, j–l and Supplementary Figs 2b–d and 5). However, this immunohistochemical method could not be used to quantify the extent of infection by AAV::GluClβ–YFP in PKC-δ::GluClαCFP-iCre transgenic mice, because of cross-reactivity of the anti-GFP antibody with the transgene-encoded CFP. The fraction of virally infected PKC-δ$^+$ neurons in PKC-δ::GluClαCFP-iCre transgenic brains was therefore estimated by quantifying the number of cells expressing intrinsic YFP fluorescence (which could be spectrally distinguished from the endogenous CFP fluorescence of the GluClα transgene). However, because this intrinsic fluorescence signal underestimates the extent of viral infection in perfusion-fixed tissue (see above), we constructed a standard curve by using wild-type mice infected with AAV:GluClβ–YFP virus, in which the number of infected cells measured by using native YFP fluorescence was plotted against the number of infected PKC-δ$^+$ cells measured by using double-immunofluorescence staining with anti-GFP and anti-PKC-δ antibodies (Supplementary Fig. 10). This standard curve was then used to estimate the fraction of PKC-δ$^+$ cells that would have been detectable by direct immunofluorescence labelling for GFP, on the basis of the quantification of native YFP fluorescence. In the behavioural experiments in which wild-type and PKC-δ::GluClα- CFP-iCre transgenic animals were classified on the basis of their infection rates (Table 1, Supplementary Table 5 and Supplementary Figs 5 and 7), this estimation method was applied to all experimental groups, including wild-type animals.

Electrophysiological slice recordings. Standard mouse brain slice preparation and whole-cell recording were performed as described[14]. In brief, coronal sections 250 µm thick were prepared with a Vibratome (VT1000S; Leica), using ice-cold glycerol-based artificial cerebrospinal fluid (composition in mM: 252 glycerol, 1.6 KCl, 1.2 NaH_2PO_4, 1.2 $MgCl_2$, 2.4 $CaCl_2$, 18 $NaHCO_3$, 11 glucose, oxygenated with 95% O_2/5% CO_2). Slices were allowed to recover for at least 1 h at 32 °C and kept at room temperature in standard artificial cerebrospinal fluid (ACSF; composition in mM: 126 NaCl, 1.6 KCl, 1.2 NaH_2PO_4, 1.2 $MgCl_2$, 2.4 $CaCl_2$, 18 $NaHCO_3$, 11 glucose, oxygenated with 95% O_2/5% CO_2). Cells expressing CFP or YFP were detected by infrared differential interference contrast and fluorescence video microscopy (Olympus BX51). Whole-cell voltage and current recordings were performed at 30 °C with a MultiClamp 700B amplifier and Digidata 1440A (Molecular Devices). The patch pipette, with a resistance of 5–8 MΩ, was filled with an intracellular solution containing (in mM) 135 potassium gluconate, 5 EGTA, 0.5 $CaCl_2$, 2 $MgCl_2$, 10 HEPES, 2 MgATP and 0.1 GTP, pH 7.2, 280–300 mosM. Data were sampled at 10 kHz, filtered at 3 kHz and analysed with pCLAMP 10 software.

Electrophysiological characterization of PKC-δ$^+$ cells. The relation of genetic marker and electrophysiological type was analysed with Fisher's exact test with the null hypothesis that PKC-δ$^+$ cells have the same proportion of late-firing neurons as do CEl neurons as a whole. We recorded 38 CEl neurons without knowing their genetic subtypes, 21 of which were late-firing neurons; 14 of the 17 non-late-firing neurons were regular spiking cells, and 3 were low-threshold bursting cells (Supplementary Tables 2 and 3). We also recorded 57 PKC-δ$^+$ neurons on the basis of their CFP expression, and found 49 of them to be late-firing neurons and 8 of them to be non-late-firing neurons (all eight of these cells were regular spiking cells; Supplementary Table 4). Fisher's exact test revealed

that PKC-δ^+ neurons have a relatively homogeneous electrophysiological property of late-firing neurons in comparison with CEl neurons as a whole.

Stereotaxic surgery. Male mice 2–4 months old were deeply anaesthetized with either ketamine/xylazine or isoflurane, injected intraperitoneally with 500 µl of 20% mannitol (Phoenix Pharmaceuticals) and placed in a stereotaxic frame (Kopf). The skull was exposed and perforated with a stereotaxic mounted drill at the desired coordinates (Supplementary Table 6). For postoperative care, mice were injected intraperitoneally with ketoprofen (2 mg per kg body weight) and supplied for 10 days with drinking water containing 80 mg l^{-1} trimethoprim, 400 mg l^{-1} sulphamethoxazole and 200 mg l^{-1} ibuprofen.

Viral injections. Viral particles were delivered unilaterally by stereotaxic (see above) injection with through stereotaxic mounted motor-driven 32-gauge 45° bevelled steel cannulas (Micro 4 controller equipped with Hamilton system; World Precision Instruments) or glass capillaries (Micro4 controller equipped with Microject system; World Precision Instruments) to one to four injection sites per hemisphere at flow rates of 50–100 nl min^{-1}.

Pharmacogenetic silencing *in vitro*. Mice were unilaterally injected with a total of 2 µl of AAV GluClα or GluClβ virus (serotype 2; (1–10) × 10^{12} particles ml^{-1} in PBS) into the central amygdala (see above). Four weeks after surgery, slices (see above) were perfused for 20 min with 20 nM ivermectin in ACSF to induce pharmacogenetic silencing.

Pharmacogenetic silencing *in vivo*. Mice were injected bilaterally with a total of 2 µl of AAV GluClα or GluClβ virus (serotypes 2, 5 and 8; (1–10) × 10^{12} particles ml^{-1} in PBS) into the central amygdala (see above). Four weeks after surgery, on day 1, animals were habituated for 20 min to context A and given a single intraperitoneal dose of 1% ivermectin injectable solution (Phoenix) at 10 mg per kg^{-1} body weight, or vehicle. On day 2, animals were fear-conditioned in context A connected to a shock scrambler (Coulbourn Scientific or Med Associates fear conditioning systems were used). After 20 min, mice were exposed to training trials of tone (85 dBA, 2 kHz) for 20 s, immediately followed by a foot shock (0.5 mA) for 2 s, with an inter-trial interval of 198 s. To avoid masking of the consequences of the experimental manipulation by ceiling and floor effects, the number of training trials (three to six) was adjusted such that freezing levels averaged about 50% in the genetic/viral control. During the training session, behaviour was recorded with infrared sensors (Coulbourn fear conditioning system) or video cameras (Med Associates fear conditioning system). On day 3, mice were placed in context B, differentiated from context A by a modified wall, floor and ceiling. Before each trial, all surfaces were cleaned with water and disinfectant. After a 5-min baseline period, two test trials of a 30-s CS followed by a 1-min post-CS period were presented. Freezing was recorded with video cameras and scored either manually by an observer blind to the experimental group of the animal (Coulbourn fear conditioning system) or electronically (Med Associates fear conditioning system). Freezing during the CS and post-CS periods are represented as bins of these two test trials. Baseline freezing was averaged over 3 min before the first CS presentation.

To investigate the relationship between freezing and the extent of viral infection (Supplementary Fig. 5a–c), freezing data were correlated with the fraction of PKC-δ^+ expressing GluClβ, estimated as described above with native fluorescence for YFP and the standard curve in Supplementary Fig. 10.

To investigate differences in freezing between experimental and control groups, freezing in the experimental group was compared with genetic/viral control groups by a two-way ANOVA with infection rate as the blocking variable (Supplementary Table 5 and Supplementary Fig. 5d–f).

Retrograde tracing with CTB. CTB (0.5% in PBS; List) was delivered by stereotaxic (see above) iontophoresis with a positive-pulsed current of 5 µA for 2 min. The animals were killed 1 week after injection, and the brains were processed for IHC.

Optogenetic circuit dissection. Mice were unilaterally injected with a total of 2 µl of Cre-dependent AAV ChR2 virus (serotypes 2 and 5; (1–10) × 10^{12} particles ml^{-1} in PBS) into the central amygdala (see above). Slices (see above) were stimulated with an optic fibre (200 µm core diameter; ThorLabs) coupled to a 473-nm laser (CrystaLaser) and mounted on a three-dimensional micromanipulator (MPC365; Sutter) with the fibre end positioned on the edge of CEl.

Cre-dependent monosynaptic tracing with rabies virus. Cre-expressing cells were primed for subsequent infection and monosynaptic retrograde spread of EnvA-pseudotyped, glycoprotein gene-deleted rabies virus, by stereotaxic injection (see above) of 180 nl of Cre-dependent AAV expressing the avian receptor protein TVA and rabies B19 glycoprotein (AAV9-pEF1α-FLEX-GTB) into the central amygdala. The genomic structure of AAV9-pEF1α-FLEX-GTB is L_ITR-EF1α Pro-Kozak-(FLEX cassette[48] containing GFP-T2A-hTVA-E2A-hB19G)-STOP-WPRE-polyA-R_ITR. The start ATG has been deleted from all three genes, and transcription start is mediated by a Kozak sequence that precedes the FLEX cassette[49]. Genes were linked together through the use of 2A elements, which permit the expression of multiple genes under the control of a single promoter[50,51]. Both the TVA and B19G genes were codon-optimized for expression in mammalian cells. The virus was prepared through a crude lysate extraction of transfected 293T cells, and had a genomic titre of 10^8 particles ml^{-1}. Although reverse-complemented GFP is detectable in the AAV genome, Cre-expressing cells expressed undetectable levels of GFP, either through native fluorescence or antibody-amplified imaging, whereas TVA and B19G appeared to express normally.

Three weeks later, mice were injected at the same site with 180 nl of glycoprotein gene-deleted rabies virus[52] that had been pseudotyped with the avian sarcoma leucosis virus glycoprotein EnvA[40]. The glycoprotein gene had been replaced with mCherry. The resulting virus, (EnvA)SAD-dG-mCherry, was incapable of infecting mammalian neurons in the absence of its binding partner, TVA, and could not spread retrogradely in the absence of the rabies B19 glycoprotein[39]. The biological titre of 10^9 particles ml^{-1} was determined through infection of TVA-expressing 293T cells. One week after the second injection, the animals were killed and the brains were processed for IHC.

Pharmacogenetic silencing with *in vivo* electrophysiological recordings. Mice were injected bilaterally with a total of 2 µl of AAV GluClα virus (serotype 2; (1–10) × 10^{12} particles ml^{-1} in PBS) into the central amygdala (see above). Four weeks later, on day 1, mice were habituated to four CS presentations (total CS duration 30 s, consisting of 50-ms pips repeated at 0.9 Hz, 2-ms rise and fall; pip frequency 7.5 kHz, 80 dB sound pressure level) in context B. On day 2, mice were conditioned with five CS/unconditioned stimulus (0.6 mA, 1 s) pairings with inter-trial intervals of 20–180 s in context A (Coulbourn fear conditioning system). On days 3, 6 and 8, mice were exposed to four CS presentations in context B. During these periods, individual neurons were recorded extracellularly in freely behaving mice. Spikes of individual neurons were sorted by time–amplitude window discrimination and template matching as described previously[53,54]. Cluster quality was verified by quantifying the cluster separation[54] (Supplementary Fig. 8). Unit isolation was verified by using autocorrelation and cross-correlation histograms. Spike rasters and histograms were constructed by aligning sweeps relative to the CS onset, and CS-evoked responses were normalized to baseline activity using a *Z*-score transformation. Detailed methodological information about *in vivo* single-unit recordings of central amygdala neurons is presented in ref. 16.

47. Gong, S., Yang, X. W., Li, C. & Heintz, N. Highly efficient modification of bacterial artificial chromosomes (BACs) using novel shuttle vectors containing the R6Kγ origin of replication. *Genome Res.* **12,** 1992–1998 (2002).
48. Atasoy, D., Aponte, Y., Su, H. H. & Sternson, S. M. A. FLEX switch targets Channelrhodopsin-2 to multiple cell types for imaging and long-range circuit mapping. *J. Neurosci.* **28,** 7025–7030 (2008).
49. Seidler, B. *et al.* A Cre-loxP-based mouse model for conditional somatic gene expression and knockdown *in vivo* by using avian retroviral vectors. *Proc. Natl Acad. Sci. USA* **105,** 10137–10142 (2008).
50. Furler, S., Paterna, J. C., Weibel, M. & Bueler, H. Recombinant AAV vectors containing the foot and mouth disease virus 2A sequence confer efficient bicistronic gene expression in cultured cells and rat substantia nigra neurons. *Gene Ther.* **8,** 864–873 (2001).
51. Szymczak, A. L. *et al.* Correction of multi-gene deficiency *in vivo* using a single 'self-cleaving' 2A peptide-based retroviral vector. *Nature Biotechnol.* **22,** 589–594 (2004).
52. Etessami, R. *et al.* Spread and pathogenic characteristics of a G-deficient rabies virus recombinant: an *in vitro* and *in vivo* study. *J. Gen. Virol.* **81,** 2147–2153 (2000).
53. Herry, C. *et al.* Switching on and off fear by distinct neuronal circuits. *Nature* **454,** 600–606 (2008).
54. Nicolelis, M. A. *et al.* Chronic, multisite, multielectrode recordings in macaque monkeys. *Proc. Natl Acad. Sci. USA* **100,** 11041–11046 (2003).